J|A|C|S
COMMUNICATIONS

Published on Web 05/09/2007

Magnesium Nanowires: Enhanced Kinetics for Hydrogen Absorption and Desorption

Weiyang Li, Chunsheng Li, Hua Ma, and Jun Chen*

Institute of New Energy Material Chemistry, Nankai University, Tianjin 300071, People's Republic of China

Received February 25, 2007; E-mail: chenabc@nankai.edu.cn

Magnesium dihydride (MgH_2) contains 7.6 wt % hydrogen, making it one of the most attractive hydrogen storage materials. However, the limitation of MgH_2 for practical application primarily lies in the sluggish hydrogen desorption kinetics and the relatively high operation temperature (about 603 K).[1,2] To overcome these drawbacks, most studies have been focused on the preparation of Mg nanoparticles and nanocomposites by high-energy ball-milling Mg/MgH_2 with appropriate elements, alloys, or compounds.[3−6] Although some doping or alloying techniques are able to affect the desorption temperature, this is always accompanied by a lower hydrogen storage capacity owing to the oxidation of Mg and the added weight. Moreover, the milling technique is limited to grain sizes down to 100 nm for pure Mg. Recently, theory calculations indicate that both Mg and MgH_2 become less stable with decreasing cluster size.[7] Experimentally, Mg nano/mesoscale (spheres, flakes, rods, and sea-urchinlike) structures have shown promising properties for application in Mg/air batteries.[8] It is thus aiming at increasing the absorption/desorption rates and lowering the desorption temperature that we here report on the preparation of Mg nanowires with different diameters and their enhanced kinetics for reversible hydrogen absorption and desorption.

The Mg nanowires were prepared by a vapor-transport approach using commercial Mg powders[8] with modified experimental setup (Figure S1, Supporting Information) that follows. First, a piece of stainless screen mesh (1500 count at the area of 10 × 10 mm^2) was used as the deposition substrate and positioned at the cooler region of the stainless-steel tube in the furnace. Second, the evaporation temperature was fixed at 1203 K with a heating time of 100 min and a flow rate of argon gas (200−400 $cm^3 \cdot min^{-1}$); while the products were deposited on the substrate at a temperature of 573 K. Third, three kinds of Mg nanowires with different diameters were obtained at the flow rates of the argon gas: 200 $cm^3 \cdot min^{-1}$ for sample 1, 300 $cm^3 \cdot min^{-1}$ for sample 2, and 400 $cm^3 \cdot min^{-1}$ for sample 3. Finally, the products on the substrate were collected through a vibratory screen separator with the protection of ultrahigh-purity Ar gas flows, allowing the substrate to be reused. The as-prepared samples were characterized by powder X-ray diffraction (XRD, Rigaku D/max-2500 X-ray generator, Cu Kα radiation), scanning electron microscopy (SEM, Philips XL-30 and JEOL JSM-6700F Field Emission), transmission electron microscopy (TEM) and high-resolution TEM (HRTEM) (FEI Tecnai 20, 200kV), and Brunauer−Emmett−Teller (BET) nitrogen adsorption−desorption measurements (Shimadzu-Micromeritics ASAP 2010). The hydrogen storage was carried out by using computer-controlled gas reaction controller apparatus (Advanced Materials Corporation)[9] and Hiden Isochema (IGA 001, Hiden Analytical Ltd)[10] with ultrahigh-purity hydrogen (99.999% pure).

Figure 1 panels a and b show the representative SEM images of the as-synthesized Mg nanowires (sample 1). From Figure 1a, it can be observed that a large number of nanowires are distributed homogeneously over a wide area, indicating that a significant proportion (over 95%) of the sample is present in a long, uniform, wirelike structure. The length of the nanowires is about several micrometers. A higher magnification SEM image (Figure 1b) displays that the nanowires have a uniform diameter of 30−50 nm. Shown in Figure 1 panels c and d are the SEM images of sample 2 at different magnifications, from which it can be seen that the nanowires are tangled together and appear to have a zigzag morphology. Figure 1d clearly reveals that the diameter of sample 2 is in the range of 80−100 nm, which is thicker than that of sample 1. Then, when the flow rate of argon gas was increased to 400 $cm^3 \cdot min^{-1}$, short and rodlike structures (sample 3) with diameters in the range of 150−170 nm were formed (Figure 1 panels e and f). Further insight into the morphology and microstructure of sample 1 by TEM (Figure 1 panels g and h) and HRTEM (Figure 1i) shows that the surface of the nanowire is roughing and that clear fringes with an interplanar spacing of 0.26 nm, which corresponds to the separation between (002) lattice planes, are aligned perpendicular to the longitudinal direction of the wire, suggesting that the nanowires grow along the [001] direction.

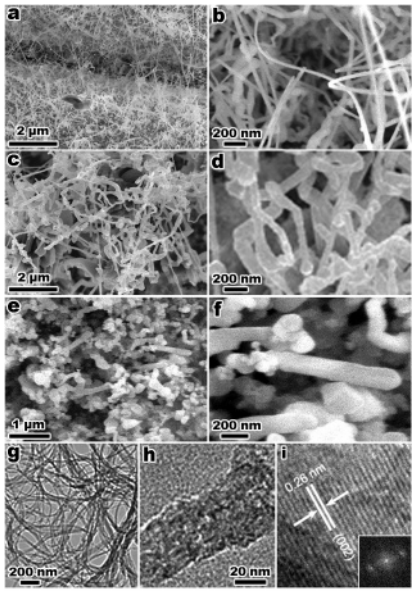

Figure 1. SEM images of the Mg nanowires: sample 1 (a, b), sample 2 (c, d), sample 3 (e, f); TEM (g, h), and HRTEM (i) images of sample 1 with the corresponding fast Fourier transform (FFT) pattern (inset).

XRD patterns of the three as-prepared Mg products (Figure S2) show that all the diffraction peaks can be indexed to the hexagonal close-packed structure of Mg (ICDD-JCPDS card no. 35-0821). The specific surface areas of samples 1, 2, and 3 are 136, 107, and 69 m^2/g, respectively (Figure S3). These high specific surface areas are due to the character of surface roughening of the nanowires.

Figure 2 illustrates the hydrogen absorption and desorption kinetics of the as-prepared Mg nanowires at different temperatures

10.1021/ja071323z CCC: $37.00

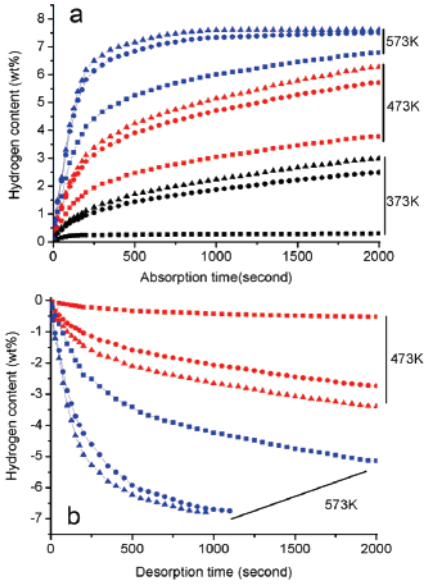

Figure 2. Hydrogen absorption (a) and desorption (b) of the Mg nanowires (sample 1, triangle; sample 2, circle; sample 3, square) at different temperatures (373 K, black; 473 K, red; 573 K, blue).

and in the hydrogen-pressure range of 0.4−2.0 MPa for absorption and 0.02−0.6 MPa for desorption. It can be seen that at each temperature the hydrogen sorption kinetics and capacities of samples 1 and 2 are significantly enhanced in comparison to those of sample 3, while sample 1 shows the fastest hydrogen absorption−desorption rates. As presented in Figure 2a, sample 1 can absorb 2.93 wt % hydrogen at 373 K with 30 min, and furthermore its hydrogen uptake at 573 K with 30 min is 7.60 wt %. During the desorption process (Figure 2b), a hydrogen release as high as 3.28 and 2.65 wt % within 30 min was achieved at 473 K for samples 1 and 2, respectively, much higher than that for sample 3 (only 0.5 wt % at the same condition). When the temperature was increased to 573 K, samples 1 and 2 desorbed about 6.77 and 6.61 wt % hydrogen within 15 min, respectively, while sample 3 only desorbed 5.01 wt % hydrogen even within 30 min. Therefore, it is apparent that the sequence of the hydrogen storage properties at various temperatures from best to worst is sample 1 > sample 2 > sample 3, demonstrating that Mg nanowires with thinner diameters take the advantage of easy activation for hydrogen absorption/desorption.

The XRD patterns of the three kinds of Mg nanowires after the first absorption process at 573 K are presented in Figure S4. With respect to sample 1 and 2, all the diffraction peaks can be indexed as a single phase of β-MgH_2 ($P4_2/mnm$) (ICDD-JCPDS card no. 12-0697), revealing that samples 1 and 2 both completely transformed to β-MgH_2 during the first hydriding process, being consistent with the absorption results of Figure 2. As to sample 3, β-MgH_2 phase with a certain amount of Mg phase can be detected, indicating its lower hydrogen storage capacity than that of samples 1 and 2. The full hydriding in only one cycle is another advantage for Mg nanowires with the diameters less than 100 nm.

To understand the improved hydriding/dehydriding kinetics of the as-prepared Mg nanowires, their activation energies during the absorption/desorption were estimated by first-order reaction rate after fitting the experimental data.[11] The absorption/desorption rate r, which corresponds to the hydrogen content as shown in Figure 2, takes the form of $r = -\ln(1 - x_H)$ where x_H is the reacted hydrogen content that was measured by the pressure drop (absorption) or increase (desorption) in a calibrated volume. Then, the temperature dependence of k can be correlated by the Arrhenius equation, $k = A \exp(-E/RT)$, where A is a temperature-independent coefficient, E is the apparent activation energy for absorption/desorption process, R is the gas constant, and T is the absolute temperature. The natural logarithm of this equation yields a first-order linear equation on the reciprocal temperature $1/T$, and the plot of $\ln k$ versus $1/T$ is shown in Figure S5. The activation energies of hydriding/dehydriding for samples 1, 2, and 3 are 33.5/38.8, 38.7/46.5, and 70.3/81.1 kJ/mol H_2, respectively. As to ball-milled MgH_2, $MgH_2 + Nb_2O_5$, and the low-temperature phase of Mg_2NiH_4, the activation energies are 120−142, 63−65,[3c] and ∼50 kJ/mol H_2,[12] respectively. In addition, from the slope of the van't Hoff plot (Figure S6), the ΔH for the dehydriding of the hydrided samples 1, 2, and 3 were calculated to be 65.3, 65.9, and 67.2 kJ/mol H_2, respectively, which are somewhat smaller than that of bulk MgH_2 (74 kJ/mol H_2).[1] It is noted that the nanowire topology of sample 1 was kept after 3 hydriding/dehydriding cycles (Figure S7) and collapsed into nanoparticles after 10 cycles (Figure S8). This is the major disadvantage that no nanowire can be regenerated. However, after a test of 50 hydriding/dehydriding cycles, the hydrogen storage capacity did not show any decrease. It is thus that this hydriding/dehydriding process may be a good way to obtain very fine nanoparticles of Mg/MgH_2.

In conclusion, the present results show that thinner Mg/MgH_2 nanowires have a much lower desorption energy than that of thicker nanowires or bulk Mg/MgH_2, indicating that changes in kinetics and thermodynamics are expected if the diameters of the nanowires are thinner than 30 nm. However, investigation into changing the enthalpy of the nano-Mg/MgH_2 system is still needed.

Acknowledgment. This work was supported by the National NSFC (20325102 and 50631020), 973 (2005CB623607) and 863 (2006AA05Z130) Project from China and the FP6 Hydrogen Solid Storage Activities (038941) from the European Community.

Supporting Information Available: Schematic diagram for the preparation of Mg nanowires, XRD patterns of Mg nanowires before and after the first hydriding process, BET measurements, Arrhenius plots for the hydriding and dehydriding kinetics of samples 1−3, van't Hoff curve of sample 1, TEM images of samples 1 after 3 and 10 cycles of hydriding and dehydriding. This material is available free of charge via the Internet at http://pubs.acs.org.

References

(1) Stampfer, J. F.; Holley, C. E.; Suttle, J. F. *J. Am. Chem. Soc.* **1960**, *82*, 3504.
(2) (a) Schlapbach, L.; Züttel, A. *Nature* **2001**, *414*, 353. (b) Grochala, W.; Edwards, P. P. *Chem. Rev.* **2004**, *104*, 1283.
(3) (a) Zaluska, A.; Zaluski, L.; Ström-Olsen, J. O. *J. Alloys Compd.* **1999**, *288*, 217. (b) Dehouche, Z.; Goyette, J.; Bose, T. K.; Hout, J.; Schulz, R. *Nano Lett.* **2001**, *1*, 175. (c) Huot, J.; Pelletier, J. F.; Lurio, L. B.; Sutton, M.; Schulz, R. *J. Alloys Compd.* **2003**, *348*, 319.
(4) (a) Oelerich, W.; Klassen, T.; Bormann, R. *Mater. Trans.* **2001**, *42*, 1588. (b) Barkhordarian, G.; Klassen, T.; Bormann, R. *J. Alloys Compd.* **2004**, *364*, 242. (c) Au, M. *Mater Sci. Eng. B: Solid State Mater Adv. Technol.* **2005**, *117*, 37.
(5) (a) Chen, J.; Sakai, T.; Kitamura, N.; Takeshita, H. T.; Kuriyama, N. *J. Am. Chem. Soc.* **2001**, *123*, 6193. (b) Hanada, N.; Ichikawa, T.; Fujii, H. *J. Phys. Chem. B* **2005**, *109*, 7188. (c) Yao, X.; Wu, C.; Du, A.; Lu, G. Q.; Cheng, H.; Smith, S. C.; Zou, J.; He, Y. *J. Phys. Chem. B* **2006**, *110*, 11697.
(6) (a) Gutfleisch, O.; Schlorke-de Boer, N.; Ismail, N.; Herrich, M.; Walton, A.; Speight, J.; Harris, I. R.; Pratt, A. S.; Züttel, A. *J. Alloys Compd.* **2003**, *356−357*, 598. (b) Alapati, S. V.; Johnson, J. K.; Sholl, D. S. *J Phys. Chem. B* **2006**, *110*, 8769.
(7) (a) Wang, X. F.; Andrews, L. *J. Phys. Chem. A* **2004**, *108*, 11511. (b) Rudy, W. P.; Wagemans, R. W. P.; van Lenthe, J. H.; de Jongh, P. E.; van Dillen, A. J.; de Jong, K. P. *J. Am. Chem. Soc.* **2005**, *127*, 16675.
(8) Li, W. Y.; Li, C. S.; Zhou, C. Y.; Ma, H.; Chen, J. *Angew. Chem., Int. Ed.* **2006**, *45*, 6009.
(9) (a) Chen, J.; Li, S. L.; Tao, Z. L.; Shen, Y. T.; Cui, C. X. *J. Am. Chem. Soc.* **2003**, *125*, 5284. (b) Sun, Y. G.; Tao, Z. L.; Chen, J.; Herricks, T.; Xia, Y. N. *J. Am. Chem. Soc.* **2004**, *126*, 5940.
(10) Chen, P.; Xiong, Z. T.; Luo, J. Z.; Lin, J. Y.; Tan, L. *Nature* **2002**, *420*, 302.
(11) (a) Schlapbach, L. *Hydrogen in Intermetallic Compounds II*; Springer-Verlag: Berlin, 1992. (b) Fernandez, J. F.; Sanchez, C. R. *J. Alloys Compd.* **2002**, *340*, 189.
(12) Hayashi, S. *Inorg. Chem.* **2002**, *41*, 2238.

JA071323Z